

# Evidence of enhanced magnetism in cool, polluted white dwarfs

Adela Kawka<sup>1</sup><sup>★</sup><sup>†</sup>, Stéphane Vennes<sup>2</sup>, Lilia Ferrario<sup>2</sup> and Ernst Paunzen<sup>3</sup>

<sup>1</sup> International Centre for Radio Astronomy Research - Curtin University, GPO Box U1987, Perth, WA 6845, Australia

<sup>2</sup> Mathematical Sciences Institute, The Australian National University, Canberra, ACT 0200, Australia

<sup>3</sup> Department of Theoretical Physics and Astrophysics, Masaryk University, Kotlářská 2, CZ-611 37, Czech Republic

Accepted XXX. Received YYY; in original form ZZZ

## ABSTRACT

We report the discovery of a new, polluted, magnetic white dwarf in the Luyten survey of high-proper motion stars. High-dispersion spectra of NLTT 7547 reveal a complex heavy element line spectrum in a cool ( $\approx 5200$  K) hydrogen-dominated atmosphere showing the effect of a surface averaged field of 163 kG, consistent with a 240 kG centred dipole, although the actual field structure remains uncertain. The abundance pattern shows the effect of accreted material with a distinct magnesium-rich flavour. Combined with earlier identifications, this discovery supports a correlation between the incidence of magnetism in cool white dwarfs and their contamination by heavy elements.

**Key words:** stars: magnetic fields – stars: individual: NLTT 7547 – white dwarfs – stars: abundances

## 1 INTRODUCTION

Magnetic fields are observed in white dwarfs across the whole evolutionary sequence with strengths varying from a few hundred MG down to a few kG (see Ferrario et al. 2015, for a review of magnetic white dwarfs). The incidence of magnetism within the white dwarf population remains uncertain. In magnitude limited surveys (e.g., Schmidt & Smith 1995; Kepler et al. 2013) the incidence of magnetism is  $\approx 5\%$ . In volume limited surveys of white dwarfs (e.g., Kawka et al. 2007) the incidence is estimated to be much higher (10 - 20 %). Landstreet et al. (2012) and Bagnulo & Landstreet (2018) conducted a survey of bright white dwarfs to search for weak magnetic fields and found that the incidence of fields in the  $\sim 1 - 10$  kG range is about  $6\pm 4\%$  which is higher than the 1 - 2% per decade incidence (Kawka et al. 2007) for stronger magnetic fields (100 kG - 500 MG).

Liebert & Sion (1979) argued that magnetism is more frequent among cooler, hence older white dwarfs, than in their hotter and younger counterparts. The significance of their conclusions was low due to their small sample of 7 magnetic white dwarfs out of a sample of 448 white dwarfs. Valyavin & Fabrika (1999) re-examined the correlation between incidence of magnetism and effective temperature using a larger sample of 49 magnetic white dwarfs out of a total of 1225 white dwarfs with reliable temperature estimates and concluded that the fraction of magnetic white dwarfs is indeed higher among cooler stars than among their hotter counterparts supporting the conclusions of Liebert & Sion (1979).

On the other hand a recent study of magnetic field evolution along the white dwarf cooling sequence was conducted by Ferrario et al. (2015) who plotted the magnetic field strength versus the effective temperature for a sample of over 600 white dwarfs. This plot did not show any apparent correlation between the magnetic field strength and effective temperature which led them to conclude that there is no field evolution along the white dwarf cooling track. The apparent lack of a correlation between the field incidence and the effective temperature proposed by Ferrario et al. (2015) may be an artifact of their Sloan-dominated sample, where Sloan spectra are low resolution and many have low signal-to-noise and therefore stronger magnetic fields are more likely to be detected. Whether or not field decay takes place remains an open question. However, there is clear evidence that the incidence of magnetism varies with spectral class and even possibly with age.

About a quarter of white dwarfs have atmospheres that are polluted by elements heavier than helium (Zuckerman et al. 2003, 2010). The origin of these heavy elements has been shown to be in accreted planetary or asteroidal debris (e.g., Debes & Sigurdsson 2002; Kilic et al. 2006; Jura et al. 2007; Jura 2008). Kawka & Vennes (2014) have shown that the incidence of magnetism is higher in cool, hydrogen-rich polluted (DAZ) white dwarfs. Similarly, Hollands et al. (2015) noted a higher incidence in cool, helium-rich, polluted (DZ) white dwarfs. The hot DQ class of white dwarfs also shows an enhanced magnetic field incidence (with surface averaged fields ranging from  $\sim 0.1$  up to 2.1 MG) that is close to 70% of these objects (Dufour et al. 2013).

Field geometry may provide clues to the origin of magnetic fields in white dwarf stars. García-Berro et al. (2012) predict complex geometries for magnetic white dwarfs formed via a dynamo event such as a merger, while descendants of Ap and Bp stars may

<sup>★</sup> E-mail: adela.kawka@curtin.edu.au (AK)

<sup>†</sup> Visitor at the Mathematical Sciences Institute, The Australian National University, Canberra, ACT 0200, Australia

be more likely to have simpler dipolar fields (Braithwaite & Spruit 2004). Field geometry is usually assumed to resemble a dipole or an offset dipole. However, when more detailed spectroscopic and spectropolarimetric observations are possible, these reveal that the magnetic field geometry is more complex. Using Zeeman tomography, Euchner et al. (2005) showed that HE 1045–0908, which has an average surface field strength of 16 MG, has a dominant quadrupolar field with contributions from dipolar and octupolar field geometries. The field geometry of some white dwarfs such as WD1953-011 can be modelled with a weak dipolar field ( $B_d = 178 \pm 30$  kG) and a stronger field of  $515 \pm 7$  kG localized on to a spot (Maxted et al. 2000; Valyavin et al. 2008). The hot hydrogen-rich white dwarf EUVE J0317-85.5 also appears to have an underlying field of  $\sim 185$  MG with a high field spot of  $\sim 425$  MG (Vennes et al. 2003). More recently, Landstreet et al. (2017) reported on the field topology of two magnetic white dwarfs with fields less than 200 kG, with one star (WD 2047+372) having a field topology corresponding to a simple dipole and the other (WD 2359–434) having a more complex topology with an underlying dipolar field and an overlaying quadrupolar field.

Hydrogen-rich white dwarfs develop a convection zone from effective temperatures below about 14 000 K, while helium-rich white dwarfs develop a convection zone below temperatures of about 28 000 K. The suppression of convective motion by magnetic fields in white dwarf atmospheres was first investigated by D’Antona & Mazzitelli (1975) who demonstrated that the evolutionary cooling rate of white dwarfs depends on the magnetic field strength. Convective energy transfer was also suppressed in the model atmospheres calculated by Wickramasinghe & Martin (1986) when they were investigating the effect of magnetic blanketing in white dwarfs. The hypothesis that magnetic fields suppress convection in white dwarf atmospheres was recently revisited by Valyavin et al. (2014) who found that a slow down in white dwarf cooling explains the higher incidence of magnetism among cool white dwarfs (Liebert & Sion 1979). Using radiation magnetohydrodynamic simulations Tremblay et al. (2015) proposed that convection is inhibited throughout the atmosphere by magnetic fields as low as 50 kG, but that the cooling rate will not be affected until the convection zone couples with the degenerate core. For higher masses, e.g., at  $1.0 M_\odot$  this occurs at  $T_{\text{eff}} \approx 6000$  K, for lower masses the coupling occurs at lower temperatures.

Our survey of high proper motion white dwarfs (Kawka & Vennes 2006, 2012a) has revealed several magnetic white dwarfs with effective temperatures below 6000 K, including NLTT 10480 (Kawka & Vennes 2011) and NLTT 43806 (Zuckerman et al. 2011). NLTT 7547 was identified as a cool, polluted white dwarf by Kawka & Vennes (2012a). In this paper we show that NLTT 7547 also harbours a magnetic field and contributes to the growing sample of magnetic cool DAZ white dwarfs. In section 2 we present the spectroscopy and photometry of NLTT 7547 and in section 3 the analysis of our results, followed by a discussion in section 4 and a summary in section 5.

## 2 OBSERVATIONS

The following section describes all available observations of NLTT 7547 and WD 0141-675. Table 1 lists the astrometric and photometric measurements.

### 2.1 Spectroscopy

We first observed NLTT 7547 with the FORS1 spectrograph attached to the Very Large Telescope (VLT) of the European Southern Observatory (ESO) at Paranal. We used the 600 lines  $\text{mm}^{-1}$  grism (Grism 600B) centred at  $4650 \text{ \AA}$  and set the slit width to 1 arcsec providing a resolution of  $\sim 6 \text{ \AA}$ . The observations were obtained on UT 2007 December 13 and conducted in the spectropolarimetric mode where we first obtained an exposure with the retarder plate rotated to  $-45^\circ$  immediately followed by an exposure with the Wollaston prism rotated to  $+45^\circ$ . These datasets were already published as part of a spectropolarimetric survey in Kawka & Vennes (2012a).

The FORS1 spectra revealed NLTT 7547 to be a cool DAZ white dwarf, and therefore, we obtained a second set of observations with the X-shooter spectrograph (Vernet et al. 2011) attached to the VLT at ESO. We obtained six sets of spectra between UT 2015 August 24 and September 19 where we set the slit-width to 0.5, 0.9 and 0.6 arcsec for the UVB, VIS and NIR arms, respectively. The exposure times for each visit were 2940, 3000 and five  $\times$  600 sec for UVB, VIS and NIR arms respectively. This setup provided a resolving power of 9760, 7410 and 8040 for the UVB, VIS and NIR arms, respectively.

We also retrieved archival spectrum of the newly identified cool DAZ WD 0141-675, which will contribute to our study of incidence of magnetism in cool DAZ white dwarfs. The spectrum was obtained with the X-shooter spectrograph on UT 2017 July 27. The slit-width was set to 1.6, 1.5 and 1.2 arcsec for the UVB, VIS, and NIR, respectively, with a nominal resolution of  $\sim 3000$ . However the spectra were taken with an average seeing of  $\sim 0.5$  arcsec at  $5000 \text{ \AA}$  and therefore we will assume a resolution of  $R \approx 5000$ . The exposure times were  $4 \times 390$ ,  $4 \times 300$  and  $4 \times 220$  sec for UVB, VIS and NIR arms respectively.

### 2.2 Photometry

We collected photometric measurements from various surveys. The Sloan Digital Sky Survey (SDSS) provided optical photometry in *u, g, r, i* and *z* bands (Albaret et al. 2017) and the Two Micron All Sky Survey (2MASS) provided infrared photometry in *J, H* and *K* bands (Skrutskie et al. 2006). NLTT 7547 was not detected by the Galaxy Evolution Explorer (GALEX).

Finally, we obtained photometric time series of NLTT 7547 in *R* using the 1.54 m telescope at La Silla. The series were obtained on UT 2017 October 18 and UT 2018 January 5. The first set of observations covered 404 minutes and the second set covered 205 minutes. The exposure times were 60 seconds for all observations at a cadence of one exposure every 78 seconds. Two comparison stars which were checked for variability were used to conduct differential photometry of NLTT 7547.

## 3 ANALYSIS

In this section we describe the model atmospheres that we use to interpret the optical spectra and thus derive the stellar parameters, the magnetic field strength and structure, and the abundance pattern. We also searched for possible spectroscopic and photometric variations.

**Table 1.** Astrometry and photometry

Parameter	Measurement	Reference
RA (J2000)	02 17 19.63	1
Dec (J2000)	-06 56 28.86	1
$\mu_\alpha \cos \delta$ (″yr <sup>-1</sup> )	0.3907 ± 0.0055	1
$\mu_\delta$ (″yr <sup>-1</sup> )	0.0143 ± 0.0055	1
$\mu_\alpha \cos \delta$ (″yr <sup>-1</sup> )	0.4225 ± 0.0003	2
$\mu_\delta$ (″yr <sup>-1</sup> )	0.0179 ± 0.0002	2
$\pi$ (mas)	22.553 ± 0.162	2
$u$	19.679 ± 0.037	3
$g$	18.318 ± 0.007	3
$r$	17.747 ± 0.006	3
$i$	17.528 ± 0.007	3
$z$	17.454 ± 0.014	3
$G$	17.800 ± 0.002	2
$b_p$	18.258 ± 0.032	2
$r_p$	17.218 ± 0.032	2
2MASS $J$	16.636 ± 0.133	4
2MASS $H$	16.182 ± 0.216	4
2MASS $K$	15.674 ± 0.251	4

References: (1) Salim & Gould (2003); (2) Brown et al. (2018); (3) Albareti et al. (2017); (4) Skrutskie et al. (2006)

### 3.1 Models

The model atmospheres assume convective equilibrium and line blanketing by dominant elements (Kawka & Vennes 2012b). Convection may be suppressed as needed. We introduced in the spectral synthesis a dipolar field distribution following Martin & Wickramasinghe (1984) and Achilleos & Wickramasinghe (1989). The dipole of strength  $|B_p|$  may be offset along the polar axis by a fraction of the radius  $a_z$  and inclined with respect to the viewer at an angle  $i$ . The visible surface is discretized in 450 elements with 30 individual latitudes between 0 and 180° and, assuming field symmetry about the meridian, 15 longitudes between 0 and 90° each counting for 2 elements. The local spectra were computed for each element. The surface-integrated spectrum is the sum of individual spectra, weighted by a linear limb-darkening coefficient.

Using convective models as an input we gradually suppressed the calculated convective flux in the models until it fell below 0.1% of the total flux hence generating radiative atmospheres. In the process, the relatively shallow convective temperature gradient steepened sharply in order to sustain the increasing radiative outflow. The effect is evident when plotting the temperature as a function of Rosseland optical depths (Fig. 1, lower panel). However, the resulting steep  $dT/dP$  gradient in the non-convective model depicted in Fig 1 (middle panel) required adjustment to the depth discretization by concentrating the distribution where  $dT/dP$  steepens. Fig 1 (upper panel) shows the corresponding density distribution. The non-convective models show a downturn in the density toward higher pressure which would give rise to a Rayleigh-Taylor instability. The same effect was noted in all models where convection was suppressed and further work should help elucidate the effect of these instabilities. We expect that the resulting mass motion should be accompanied by energy transfer and reduce the steepness of the temperature gradient.

The hydrogen Balmer spectra, from  $H\alpha$  to  $H\epsilon$  were computed using line strengths and Zeeman shifts from Schimeczek & Wunner (2014). We computed detailed heavy element line profiles following procedures described in Kawka & Vennes (2011) but updated using quadratic Zeeman line splitting formulae from

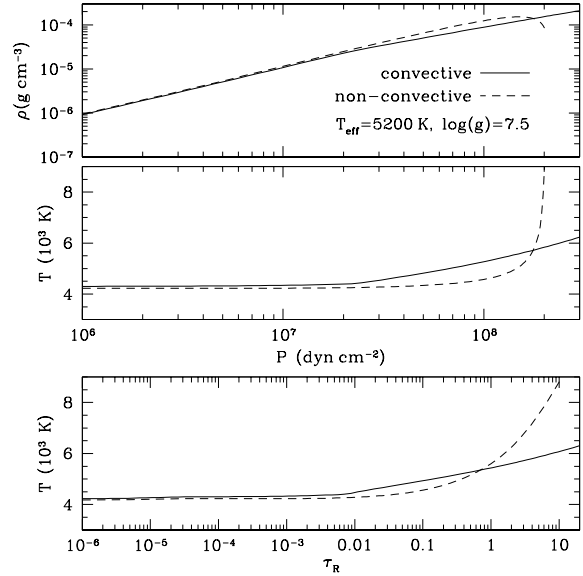


**Figure 1.** A comparison of the structure of a model atmosphere with convective energy transport (full lines) and without (dashed lines). The temperature structure of the model at 5200 K ( $\log g = 7.5$ ) is plotted as a function of optical depth (lower panel) and pressure (middle panel). The corresponding density structure is plotted as a function of pressure (upper panel).

Landi Degl’Innocenti & Landolfi (2004). The updated Zeeman patterns agree with earlier calculations for Ca II H&K lines which employed the tabulation of Kemic (1975).

Given the low effective temperature of NLTT 7547, we tested whether the population of molecules, such as NaH, MgH, AlH, CaH, and FeH, is high enough to affect the abundance measurements of the atomic species. We conducted the tests in both convective and non-convective atmospheres. In our calculations we have used the partition functions of Sauval & Tatum (1984), Wende et al. (2010) and Barklem & Collet (2016) with the FeH dissociation energy of 1.69 eV (Cheng et al. 2017). We found that abundance measurements can differ by up to 10% by including either MgH, AlH or FeH and about 1% by including NaH or CaH. We inspected the NIR spectrum and did not detect FeH in the 999 to 1000 nm range (see, e.g., Wende et al. 2010) although a spectral synthesis of FeH bands in cool, hydrogen-rich white dwarfs has not been included in the present work.

### 3.2 Stellar parameters

As a result of these recent studies, we have re-analysed the atmospheric properties of NLTT 7547 using two sets of hydrogen-rich model atmospheres. The first set consists of fully convective models and these are described in Kawka & Vennes (2006) and Kawka & Vennes (2012b), however in these sets of models we have multiplied the self-broadening parameter,  $\Gamma_{BPO}$ , from Barklem et al. (2000) by 1.0 rather than by 0.75 which was initially adopted in the calculations of Kawka & Vennes (2012b) in order to secure a mean sample mass of  $0.6 M_\odot$ . We then computed an additional set of model atmospheres and spectra where convection is suppressed and therefore energy is carried radiatively.

Figure 2 shows the best-fitting synthetic Balmer lines compared to the X-shooter spectra for models including convection and, separately, for models that suppress convection. Using the convective models, we fitted the observed Balmer lines ( $H\alpha$ ,  $H\beta$

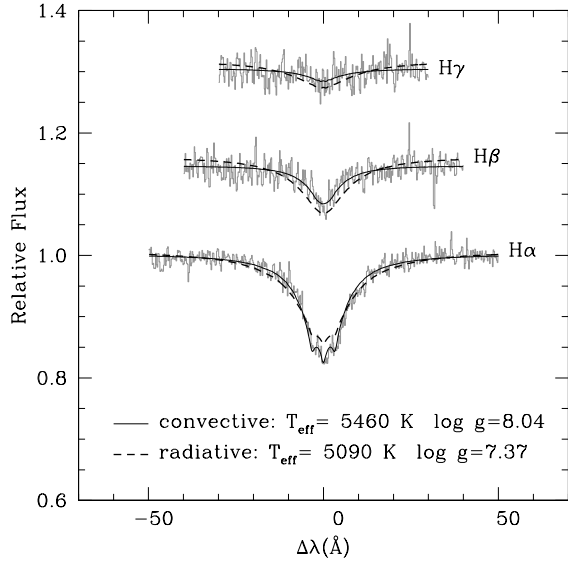


**Figure 2.** Balmer line profiles showing Zeeman splitted cores of NLTT 7547 compared to the best fitting model spectrum with convection (solid lines) and convection fully suppressed (dashed lines).

and  $H\gamma$ ) of NLTT 7547 in the surface gravity ( $\log g$ ) versus effective temperature ( $T_{\text{eff}}$ ) plane and obtained  $T_{\text{eff}} = 5460 \pm 80$  K and  $\log g = 8.04 \pm 0.18$ . Using the non-convective models we obtained  $T_{\text{eff}} = 5090 \pm 100$  K and  $\log g = 7.37 \pm 0.22$ . However the calculated Balmer lines in the radiative models are poorly matched to the observed lines, particularly in the core. The superior goodness of fit of convective models relative to non-convective models ( $\chi_{\text{R,nc}}^2 / \chi_{\text{R,c}}^2 = 1.4$ ), which in principle is sufficient to reject non-convective models, may be an artifact of the line-broadening prescription. Bédard et al. (2017) analysed three magnetic white dwarfs with effective temperature below 9000 K, and showed that in these cases convective models were preferred and concluded that at lower effective temperatures it may be more difficult for a weak field to suppress convection. However, the validity of our simple line broadening prescription upon which our results are based remains to be confirmed in the presence of a  $\approx 10^6$  G magnetic field.

Next, we fitted the spectral energy distribution (SED) in the  $T_{\text{eff}} - \log g$  plane using available optical and infrared photometry. We constrained the synthetic magnitudes by using the Gaia parallax (Table 1) to set the distance  $D$  and by applying mass-radius relations from Benvenuto & Althaus (1999) to set the stellar radius  $R$  in the ratio  $R^2/D^2$ . Figure 3 shows the observed photometric measurements from SDSS and 2MASS compared to the best fitting synthetic photometry. Using convective models we obtained  $T_{\text{eff}} = 5198 \pm 54$  K which is more than 200 K lower than the effective temperature determined from the Balmer line fits. These results differ significantly and a similar disagreement between the effective temperature determined from Balmer lines and from the SED was encountered in the analysis of the cool DAZH NLTT 10480 (Kawka & Vennes 2011). Nearly identical parameters are obtained using radiative models but with a poorer goodness of fit. Figure 3 shows the observed SED compared to the best fitting synthetic photometry at  $T_{\text{eff}} = 5108 \pm 128$  K. After excluding the SDSS  $u$  and 2MASS  $K$  bands which deviate most from the synthetic photometry we find the reduced  $\chi^2$  for non-convective models  $\chi_{\text{R,nc}}^2 > 5$  while for convective models  $\chi_{\text{R,c}}^2 \approx 0.5$ . The excess in the  $K$  band may indicate the presence of circumstellar dust at a lower tem-

perature than in any previous detections near white dwarfs (see, Farihi, Zuckerman & Becklin 2008).

In summary, the Balmer lines and SED results are not mutually consistent using either convective or non-convective models. On the other hand synthetic Balmer line profiles and synthetic SED computed with convective models fit significantly better the data.

We have calculated the Galactic velocity vectors of NLTT 7547 using the method of Johnson & Soderblom (1987) and the correction for the Solar motion from Hogg et al. (2005). As input we have used the distance and proper motion from Gaia and we measured a barycentric corrected velocity of  $v = -16.9$  km s $^{-1}$  from the spectral lines in the X-shooter spectra. NLTT 7547 has components  $U, V, W = -44, -53, 52$  km s $^{-1}$  which are representative of a thick disc velocity (Soubiran et al. 2003). We have used Rossi (2015) to calculate the z-component of the angular momentum ( $J_z$ ) and the eccentricity ( $e$ ) of NLTT 7547. Following Pauli et al. (2003),  $J_z = 1420$  kpc km s $^{-1}$  and  $e = 0.262$  place NLTT 7547 between thin and thick disc Galactic orbits, making NLTT 7547 part of the old disc population.

Adopting the mass and radius constrained by the Gaia parallax in the SED analysis (Table 3), the white dwarf cooling age is 3.1-4.3 Gyr. The age of the thick disc has been estimated at 9.5-9.9 Gyr using white dwarf luminosity function (Kilic et al. 2017) or 10-13 Gyr based on cluster isochrones (e.g., 47 Tuc, Liu & Chaboyer 2000; Salaris et al. 2007). The lifetime of the progenitor would then extend between 6 to 10 Gyr corresponding to a mass of 1.1 down to  $0.95 M_{\odot}$  using evolutionary models with a low metallicity ( $Z = 0.004$ , see a tabulation in Romero et al. 2015) comparable to that of 47 Tuc. The initial mass ( $0.95$ - $1.1 M_{\odot}$ ) and the corresponding final mass ( $0.50$ - $0.54 M_{\odot}$ ) fit well within the initial-to-final mass relations devised by, e.g., Ferrario et al. (2005) and Romero et al. (2015).

Tremblay et al. (2015) showed that the convection zone couples with the degenerate core at an effective temperature of 5527 K for a  $0.6 M_{\odot}$  white dwarf thereby increasing its energy release for a certain period of time. During that period of time the cooling age of the non-magnetic (i.e., convective) white dwarf is effectively longer than that of its magnetic (i.e., with convection suppressed) counterpart with the same effective temperature. But having exhausted its internal energy faster, the non-magnetic white dwarf catches up with its magnetic counterpart by the time they both reach a temperature of 3340 K. At this stage the cooling rate of magnetic white dwarfs decreases compared to the cooling rate of non-magnetic white dwarfs. Below a temperature of 3340 K the roles are inverted and the cooling age of the magnetic white dwarf becomes increasingly longer compared to a non-magnetic white dwarf with the same effective temperature.

At a lower mass of  $0.52 M_{\odot}$  appropriate for NLTT 7547, the coupling would occur at a temperature lower than 5527 K and possibly as low as a temperature of 5200 K appropriate for NLTT 7547. Therefore the cooling age of convective models would overestimate the true age of NLTT 7547 assuming that its magnetic field has suppressed the convection zone. However, the difference in the cooling times amounts to  $\lesssim 20\%$ , i.e., 0.7 Gyr.

### 3.3 Magnetic fields

Kawka & Vennes (2012a) measured a longitudinal field of  $B_l = -23.5 \pm 177.0$  kG using  $H\beta$  and  $H\gamma$  and  $B_l = -32.2 \pm 40.2$  kG using the Ca II H&K lines. The Ca II measurement has a  $1-\sigma$  upper limit of  $|B_l| \leq |72.4|$  kG. The large uncertainty in the longitudinal mag-

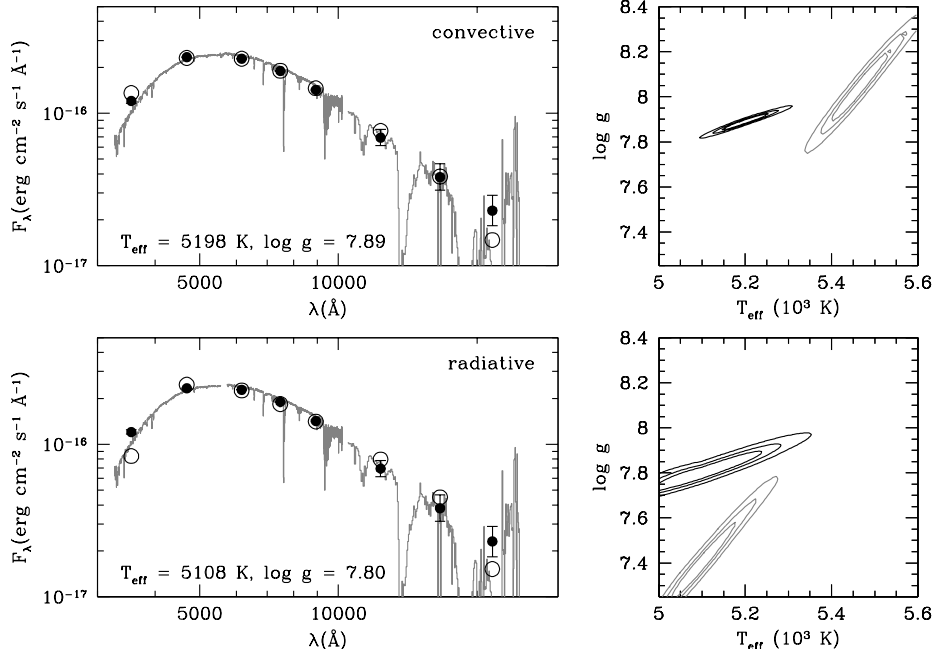


**Figure 3.** The spectral energy distribution of NLTT 7547. The photometric measurements are represented by filled circles and the best-fitting model photometric points are in open circles. The X-shooter spectrum (binned by 20 in UVB/VIS and 100 in NIR) is plotted in grey for comparison. The observed photometric points are compared to model photometry assuming a convective atmosphere (top panel) and assuming a radiative atmosphere (bottom panel). The right panels compare the 1,2 and 3- $\sigma$  contours of the SED fits (in black) and Balmer line fits (in grey).

**Table 2.** Main spectral line identification

Ion	$\lambda$ (Å)	Ion	$\lambda$ (Å)
Fe I	3719.934	Ca II	3968.469
Ca II	3736.902	Ca I	4226.728
Fe I	3737.131	H $\beta$	4861.333
Fe I	3745.561	Na I	5889.951
Mg I	3832.304	Na I	5895.924
Mg I	3838.292	H $\alpha$	6562.819
Ca II	3933.663	Ca II	8498.02
Al I	3944.006	Ca II	8542.09
Al I	3961.520	Ca II	8662.14

netic field measurement does not allow us to place constraints on the inclination of the magnetic field.

The X-shooter spectra has revealed Zeeman splitted lines of Na, Mg, Al, Ca, Fe with H Balmer lines. Table 2 lists the heavy element lines detected and their rest wavelengths.

The magnetic field of NLTT 7547 is low enough that the anomalous Zeeman splitting can be assumed for Na, Mg, Al, Ca and Fe. For details on how we calculate line splitting in this regime, see Kawka & Vennes (2011). We have measured an average surface field of  $155.7 \pm 12.4$  kG from the Ca II H line at 3933.663 Å while the Zeeman splitting in H $\alpha$  results in a surface average field of  $163 \pm 4$  kG.

Depending on the topology of the magnetic field, the lines can be broadened as a result of a field spread. We have calculated model spectra by varying the dipolar field strength ( $B_p$ ), inclination ( $i$ ) and the offset ( $a_z$ ) by a fraction of the stellar radius along the polar axis (see Vennes et al. 2018). We have found that the best fit to the data of NLTT 7547 is provided by a centred dipole ( $a_z = 0$ ) of 240 kG. A centred dipole field show broader lines due to field spread than

a more uniform field given by a substantially offset dipole. The broad line shapes of metal lines in NLTT 7547 can be best modelled by a centred dipole ( $a_z = 0$ ) of 240 kG in agreement with the H $\alpha$  modelling.

The centred dipole solution is not necessarily unique and other combinations of field strength, inclination and offset are possible. In order to investigate the likelihood of more complex field geometries, such as the presence of a magnetic spot or multipolar fields, phase resolved data are required. Without any indication of phase-dependent variations we cannot ascertain whether the star is in fact fast rotating and all measurements are surface averaged, or the star is slow rotating and, therefore, is viewed at a fixed phase angle. Consequently, the centred dipole model may not be complete, and we can only state that the broadened shape of the Ca II H&K lines is consistent with a centred dipole.

Vennes et al. (2018) revisited the cool, magnetic white dwarfs, NLTT 10480 (Kawka & Vennes 2011) and NLTT 53908 (Kawka & Vennes 2014) by modelling the magnetic field by considering different field configurations. In our previous analysis of these objects, we assumed a uniform field. A dipolar field offset away from the observer is more uniform and thus the spectral lines a less broadened. This seems to be the case for NLTT 53908 which exhibits Zeeman features that are much sharper than those yielded by a centred dipole. Our modelling indicates that the field structure is that of a dipolar field of 635 kG offset by  $a_z = -0.2$  (therefore away from the observer) along the magnetic axis and  $i = 70^\circ$ . A refit of the narrow Zeeman Ca components in NLTT 10480 has also required a large offset of  $a_z = -0.3$  for a field of  $B_p = 1.1$  MG and  $i = 70^\circ$ .

### 3.4 Abundance Analysis

We determined the abundances of Na, Mg, Al, Ca and Fe using the effective temperature and surface gravity derived by using our convective models. We calculated separately the abundances for parameters obtained using Balmer line profiles and the SED. The measured abundances are listed in Table 3.

We fitted all Ca lines, that is Ca II H&K at 3933.663 and 3968.469 Å, Ca I at 4226.728 Å and the infrared Ca II triplet at 8498.02, 8542.09 and 8662.14 Å. We could not achieve a consistent fit at the same abundance for all three sets of lines when using the atmospheric parameters from the Balmer line fits. Therefore, we fitted them separately and obtained three separate abundance measurements. For Ca II H&K we measured  $\log(\text{Ca}/\text{H}) = -10.06 \pm 0.06$ , for Ca I we obtained  $\log(\text{Ca}/\text{H}) = -9.60 \pm 0.18$  and using the Ca II infrared triplet we measured  $\log(\text{Ca}/\text{H}) = -8.91 \pm 0.23$ . The consistency between the Ca II H&K and Ca I abundance measurements was improved by decreasing the effective temperature, as was also shown by [Kawka & Vennes \(2011\)](#) in the case of NLTT 10480. The discrepancy between Ca II H&K and the infrared Ca II triplet remains unexplained.

Next, we repeated the calcium abundance measurements using the atmospheric parameters from the SED fit. Using Ca II H&K we measured  $\log(\text{Ca}/\text{H}) = -10.12 \pm 0.04$ , with Ca I we measured  $\log(\text{Ca}/\text{H}) = -9.77 \pm 0.36$ , and with Ca II infrared triplet we measured  $\log(\text{Ca}/\text{H}) = -9.31 \pm 0.35$ . These abundance measurements are more consistent with each other than with the warmer temperature derived from the Balmer line fits.

Figure 4 shows the X-shooter spectrum of NLTT 7547 compared to the best-fitting model spectrum calculated using the atmospheric parameters ( $T_{\text{eff}} = 5460$  K and  $\log g = 8.04$ ) determined from the Balmer line fit. The main lines or group of lines labelled.

NLTT 7547 is yet another example of a white dwarf accreting material from its circumstellar environment. Its composition, represented by Mg, Ca, and Fe, appears magnesium rich relative to bulk-Earth material ([Hollands, Gänsicke & Koester 2018](#)).

### 3.5 Test of variability

Using H $\alpha$  we measured a surface averaged magnetic field  $B_S = 163 \pm 4$  kG for NLTT 7547. We also measured the surface averaged magnetic field using the Ca II H&K lines. In this case we calculated model spectra at various abundances and magnetic field strengths around 163 kG, and then by fitting the observed Ca II H&K line profiles we found  $B_S = 155.7 \pm 10.5$  kG. The dipolar field strength  $B_P = 240$  kG is then constrained by the inclination and dipole offset. The resulting calcium abundance is  $\log(\text{Ca}/\text{H}) = -10.06 \pm 0.05$ . Since we obtained 6 sets of spectra over a period of less than one month, we also fitted the Ca II H&K line profiles for each observation to check for variability. The measurements are summarized in Table 4: the starting time and exposure time are for the UVB spectra and the Barrycentric Julian Date (BJD) is calculated at mid-exposure. The Ca abundance and magnetic field strength do not appear to vary. We found that the average of Ca abundance is  $\log(\text{Ca}/\text{H}) = -10.05$  with a dispersion of 0.06 and the average of the magnetic field strength is  $B_S = 155.4$  kG with a dispersion of 6.3 kG. Since the individual exposure times were 2940 sec each in the UVB arm, the white dwarf could be either a fast rotator with a rotation period less than an hour or a slow rotator with a period larger than a few months. Alternatively the field could be relatively stable as a function of the rotation phase, which would suggest very small viewing angles to the magnetic axis.

**Table 3.** Stellar and atmospheric parameters of NLTT 7547 using convective models.

Parameter	Measurement
Balmer line profiles	
$T_{\text{eff}}$ (K)	$5460 \pm 80$
$\log g$ (cgs)	$8.04 \pm 0.18$
Mass ( $M_{\odot}$ )	$0.61 \pm 0.12$
Distance (pc)	$52.8 \pm 7.0$
Age (Gyr)	$3.5 \pm 1.0$
$\log(\text{Na}/\text{H})$	$-8.57 \pm 0.08$
$\log(\text{Mg}/\text{H})$	$-7.99 \pm 0.19$
$\log(\text{Al}/\text{H})$	$-8.79 \pm 0.20$
$\log(\text{Ca}/\text{H})$	$-10.06 \pm 0.06$
$\log(\text{Fe}/\text{H})$	$-8.81 \pm 0.13$
Spectral energy distribution	
$T_{\text{eff}}$ (K)	$5198 \pm 54$
$\log g$ (cgs)	$7.89 \pm 0.04$
Mass ( $M_{\odot}$ )	$0.52 \pm 0.02$
Age (Gyr)	$3.7 \pm 0.6$
Radius ( $R_{\odot}$ )	$0.0135 \pm 0.0003$
Gaia $\pi$ (mas)	$22.55 \pm 0.16$
Gaia Distance (pc)	$44.34 \pm 0.32$
$\log(\text{Na}/\text{H})$	$-8.68 \pm 0.09$
$\log(\text{Mg}/\text{H})$	$-8.09 \pm 0.14$
$\log(\text{Al}/\text{H})$	$-9.09 \pm 0.07$
$\log(\text{Ca}/\text{H})$	$-10.12 \pm 0.04$
$\log(\text{Fe}/\text{H})$	$-8.84 \pm 0.06$
$B_S$ (kG)	$163 \pm 4$

We have used a fast Fourier transform routine to search for variations in the photometric time series obtained in the  $R$  filter, but did not yield any significant periods. Since this photometric time series was obtained during two nights, we also searched for periods in the data taken on both nights combined as well as data obtained on individual nights. To place some constraints on the variations of NLTT 7547 we measured the dispersion of the photometric measurements. On the first night (UT 18 October 2017) we measured a dispersion of  $\sigma = 0.014$  mag and on the second night (UT 5 January 2018) we measured a dispersion of  $\sigma = 0.011$  mag. The second night provided tighter constraints as a result of better observing conditions.

## 4 DISCUSSION

The studies of cool and magnetic white dwarfs have unveiled new challenges in our understanding of the atmospheric structure, formation and evolution of magnetic white dwarfs. In this section we will discuss some of the issues surrounding this class of objects.

### 4.1 Convective versus radiative energy transport

Magnetic fields have been thought to inhibit convection in cool white dwarfs. Some support for this suppression has recently come from the modelling of the weakly magnetic white dwarf WD 2105–820 ([Gentile Fusillo et al. 2018](#)) who fitted the ultraviolet and optical spectra of three non-magnetic white dwarfs with  $T_{\text{eff}}$  between 9000 and 11 000 K and the weakly magnetic WD 2105–820 with both radiative and convective models. For WD 2105–820, consistent atmospheric parameters were derived only when radiative models were used, while for the non-magnetic

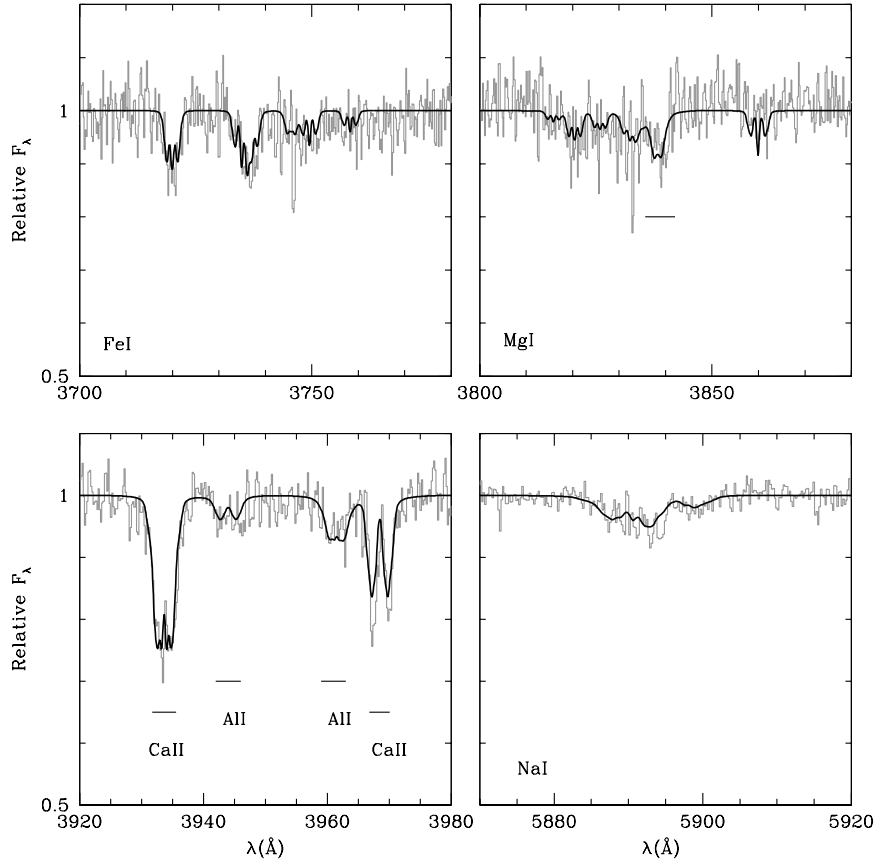


**Figure 4.** X-Shooter spectrum (grey) compared to the best fitting model spectrum (black) at  $T_{\text{eff}} = 5460 \text{ K}$  and  $\log g = 8.04$  showing the Zeeman splitted metal lines Na, Mg, Al, Ca and Fe.

**Table 4.** Calcium abundance and magnetic field measurements for individual spectroscopic observations.

UT date	UT start	Exposure time (s)	BJD (2457200+)	$\log(\text{Ca}/\text{H})$	$B_S$ (kG)
2015 August 24	09:09:35	2940	58.90153	$-10.08 \pm 0.08$	$158.1 \pm 16.5$
2015 September 10	08:09:47	2940	75.86120	$-10.12 \pm 0.11$	$144.3 \pm 30.0$
2015 September 13	08:28:18	2940	78.87424	$-9.96 \pm 0.13$	$161.5 \pm 20.5$
2015 September 17	08:30:41	2940	82.87612	$-10.11 \pm 0.09$	$156.6 \pm 21.3$
2015 September 19	05:05:32	2940	84.73375	$-10.02 \pm 0.12$	$150.0 \pm 22.7$
2015 September 19	06:17:05	2940	84.78344	$-10.02 \pm 0.11$	$150.0 \pm 22.7$

white dwarfs, consistent results were obtained with convective models. [Bédard et al. \(2017\)](#) provided independent evidence for convection suppression in WD 2105–820. Using radiative models, they were able to match the photometrically and spectroscopically determined effective temperatures and also successfully matched the spectroscopically determined distance with the measured parallax.

In the case of NLTT 7547, neither types of models successfully account for all data. Two independent diagnostics, the Balmer line profiles and the SED, provided irreconcilable stellar parameters ( $T_{\text{eff}}$ ,  $\log g$ ). However, convective models provided significantly better fits to the Balmer line profiles and the SED when analysed separately. Difficulties encountered in fitting Balmer line profiles may, in part, be caused by an inadequate line broadening

theory in cool, magnetic atmospheres. We will assume that cool, magnetic white dwarfs have convective atmospheres pending further investigations of non-convective atmospheres.

## 4.2 Field structure

[Brinkworth et al. \(2013\)](#) obtained time-photometry series of several magnetic white dwarfs and found that more than half are variable. Such white dwarfs can be used to study the magnetic field variations on the white dwarf surface as a function of rotational phase. A few magnetic white dwarfs have been observed spectropolarimetrically over their rotational period revealing the complexity of the magnetic field structure. The rapidly rotating EUVE J0317–85.5 varies photometrically, spectroscopically and

spectropolarimetrically (Barstow, et al. 1995; Ferrario et al. 1997; Burleigh et al. 1999; Vennes et al. 2003). These variations as a function of rotation phase reveal that the magnetic field structure of EUVE J0317-85.5 is rather complex and probably is a combination of a lower underlying field of  $\sim 185$  MG with a stronger magnetic field of  $\sim 450$  MG concentrated in a spot (Vennes et al. 2003). More recently, the magnetic white dwarf in the close double degenerate system NLTT 12758, showed photometric and spectropolarimetric variations as a function of the rotation phase (Kawka et al. 2017). Photometric variations NLTT 8435 with a period of 95 minutes, that is mostly likely due to rotation, was reported by Vennes et al. (2018).

Magnetic white dwarfs that do not appear to vary are either rotating with a very long period or their magnetic field is nearly aligned with the rotation axis. Photometric variations in NLTT 7547 are restricted to amplitudes below 11 mmag for periods up to  $\approx 2$  hr. In addition, we did not detect any variations in the six spectra obtained over several days, but because these spectra have exposure times close to one hour, any short period variations would be averaged out during the exposure and would remain undetected. Higher signal-to-noise photometric time series would be required to probe low-amplitude ( $< 10$  mmag), longer period ( $> 2$  hr) variations.

### 4.3 Incidence of magnetism

Recent identifications of magnetic white dwarfs suggest that the incidence of magnetism differs among different spectral classes. In the past, various surveys have been carried out to search for new magnetic white dwarfs to determine the incidence of magnetism. While colourimetric and magnitude limited surveys (e.g., Schmidt & Smith 1995; Kepler et al. 2013; Bagnulo et al. 2018) yielded an incidence of around 5%, volume limited surveys delivered fractions as high as 20% (e.g., Kawka et al. 2007).

Most of these surveys were targeted toward hydrogen-rich white dwarfs. Recent observations of different spectral classes have revealed higher incidences of magnetism in some of these classes. The highest fraction of magnetism is found in the rare class of warm and hot DQ white dwarfs. Dufour et al. (2013) reported an incidence of  $\sim 70\%$ , which may suggest that all warm/hot DQ may be magnetic. Hot DQ white dwarfs are photometrically variable with periods ranging from a few minutes up to a couple of days. These variations have been proposed to be the result of rotation (Lawrie et al. 2013; Williams et al. 2016). Dufour et al. (2013) also suggested that this group of white dwarfs are massive, and Dunlap & Clemens (2015) proposed that they may be the product of white dwarf mergers due to their rapid rotation and high mass ( $M \gtrsim 0.9 M_{\odot}$ ).

Hollands et al. (2015, 2017) have shown that the incidence of magnetism in a sample of 79 cool ( $T_{\text{eff}} < 8000$  K) DZ white dwarfs is more than 10%, which is significantly higher than the incidence observed in the overall white dwarf population. The magnetic fields in these stars range from a  $\approx 0.5$  MG to over 10 MG.

The sample of cool DAZ white dwarfs is still relatively small, but it already reveals that magnetism is more common among DAZs with  $T_{\text{eff}} < 6000$  K than in the general white dwarf population. Kawka & Vennes (2014) have shown that over 40% of DAZ white dwarfs with  $T_{\text{eff}} < 6000$  K are magnetic.

The incidence of magnetism among local ( $\leq 20$  pc) DA white dwarfs listed by Giammichele et al. (2012) is comparable ( $\approx 20\%$ ) to that of all local white dwarfs (Kawka et al. 2007). However, the magnetic DA white dwarfs in the local sample cover a much

wider range of field strengths (0.1-100 MG) than that observed in the population of magnetic DAZ white dwarfs (0.1-1 MG). Therefore, the field incidence per decade of field strength is significantly larger among DAZ white dwarfs. Note that taking into account the shorter cooling ages of magnetic white dwarfs relative to their non-magnetic counterparts only increases the significance of this excess. On the other hand, the noted absence of high-field DAZ white dwarfs in our sample underlines difficulties in detecting weak, heavily-spread spectral lines in these objects.

Here we revisit this population study with an updated census which includes the case NLTT 7547 and others. Figure 5 shows the known DAZ white dwarfs that have been observed with sufficiently high resolution ( $R = \lambda/\Delta\lambda \gtrsim 5000$ ) that can constrain weak magnetic fields well below 100 kG, while Table 5 lists the properties of objects with an effective temperature below 7000 K. We also checked if these white dwarfs were observed spectropolarimetrically, since spectropolarimetry can also reveal weak magnetic fields if observed with high enough signal-to-noise ratio. We include longitudinal magnetic field measurements or upper limits for those stars that have been observed spectropolarimetrically. Our sample has been selected from Zuckerman et al. (2003), Farihi et al. (2011), Zuckerman et al. (2011), Kawka & Vennes (2011, 2012a, 2014, 2016), Kawka et al. (2011) and Vennes & Kawka (2013). More cool DAZ white dwarfs have been discovered recently, however most of them have not been observed with sufficiently high resolution. Stars with  $T_{\text{eff}} < 7000$  K are WD2028-171 (Subasavage et al. 2017), and WD0920+012 and WD1408+029 from Sayres et al. (2012). Another cool white dwarf, but with  $T_{\text{eff}} = 7220 \pm 246$  K is WD2157-574 which was identified by Subasavage et al. (2007). Debes & Kilic (2010) reported the detection of Ca II H&K in the nearby WD0141-675. We have analysed the X-shooter spectrum of WD0141-675 using our model spectra to determine  $T_{\text{eff}} = 6150 \pm 10$  K,  $\log g = 7.58 \pm 0.02$  and  $\log(\text{Ca}/\text{H}) = -10.96 \pm 0.11$ . We have measured a velocity differential  $v(\text{Ca II}) - v(\text{H}\alpha) \approx -3 \text{ km s}^{-1}$  suggesting a photospheric origin to the calcium lines. The X-shooter spectrum does not show evidence for the presence of a magnetic field. WD 1223-659 was reported to be a new DAZ by Debes & Kilic (2010) with  $T_{\text{eff}} = 7660 \pm 220$  K (Subasavage et al. 2009). The narrow Ca II line at 3933Å shown in Debes & Kilic (2010) does not appear to show signs of a magnetic field. WD 1223-659 is included in the histogram of Fig. 5, however since there are no abundance measurements available it is excluded from the abundance plot. The figure shows that the incidence of magnetism among the coolest known DAZ white dwarfs is now closer to 50% with a significantly lower incidence at higher temperatures.

Recently, Briggs et al. (2018) discussed a possible scenario, originally proposed by Farihi et al. (2011) to explain G 77-50, which may be able to explain the higher incidence of magnetism among cool, magnetic DAZ and DZ white dwarfs. In this scenario, a gaseous planet plunges onto an aging white dwarf. The differential rotation that is set off would generate a relatively weak magnetic field in the white dwarf. It is not clear what would cause such a planet to spiral in toward the white dwarf, but Farihi et al. (2011) have proposed that outer planets and asteroids could have been destabilised by a close encounter with another stellar object during the billions of years that the white dwarf has spent orbiting around the Galaxy. Farihi et al. (2011) estimated that such an encounter has a 50 per cent probability to occur every 0.5 Gyr. Hence, the older the white dwarf, the more likely it is that it will have experienced a close stellar encounter capable of perturbing the orbits of its outer planets that were not engulfed during the progenitor

**Table 5.** Known cool DAZ white dwarfs ( $T_{\text{eff}} < 7000$  K) with mid/high-resolution spectra ( $R \geq 5000$ ).

WD	Name	$T_{\text{eff}}$ (K)	$\log g$ (c.g.s)	$\log(\text{Ca}/\text{H})$	Fe/Ca	$B_s$ (kG)	$ B_l $ (kG)	Reference
WD0015–055	NLTT 888	$5570 \pm 40$	$7.72 \pm 0.08$	$-10.77 \pm 0.06$	58	$< 40$	$< 40$	1,2
WD0028+220	NLTT 1675	$6020 \pm 50$	$8.04 \pm 0.07$	$-9.53 \pm 0.03$	8	$< 40$	...	3
WD0141–675	LTT 934	$6150 \pm 10$	$7.58 \pm 0.02$	$-10.96 \pm 0.11$	..	$< 70$	$< 16$	4,5
WD0151–308	NLTT 6390	$6040 \pm 40$	$7.90 \pm 0.07$	$-10.00 \pm 0.04$	27	$< 40$	$< 11$	2,3
WD0214–071	NLTT 7547	$5460 \pm 80$	$8.04 \pm 0.18$	$-10.01 \pm 0.05$	25	$163 \pm 4$	$< 72.4$	5
WD0243–026	LHS 1442	$6800 \pm 300$	$8.15 \pm 0.10$	$-9.90$	...	$< 10$	...	6
WD0245+541	G 174-14	$5190 \pm 300$	$8.22 \pm 0.10$	$-12.69$	...	$< 10$	...	7
WD0315–293	NLTT 10480	$5200 \pm 200$	$8.0 \pm 0.5$	$-10.3 \pm 0.3$	$< 10$	$519 \pm 4$	$212 \pm 50$	3,7
WD0322–019	G 77-50	$5310 \pm 100$	$8.05 \pm 0.01$	$-9.8 \pm 0.2$	13	120	$16.5 \pm 2.3$	8,9
WD0334–224	NLTT 11393	$5890 \pm 30$	$7.86 \pm 0.06$	$-10.24 \pm 0.04$	$< 7$	$< 40$	$< 16$	2,3
WD1208+576	G 197-47	$5830 \pm 300$	$7.91 \pm 0.10$	$-10.96$	...	$< 10$	...	6
WD1344+106	G 63-54	$6945 \pm 300$	$7.99 \pm 0.10$	$-11.13$	...	$< 10$	...	6
WD1633+433	G 180-63	$6570 \pm 300$	$8.08 \pm 0.10$	$-8.63$	5	$< 10$	...	6
WD1653+385	NLTT 43806	5900	8.0	$-7.9 \pm 0.19$	1.3	70	...	10
WD2225+176	NLTT 53908	$6250 \pm 70$	$7.87 \pm 0.12$	$-9.85 \pm 0.04$	$< 13$	$334 \pm 3$	...	1

References: (1) Kawka & Vennes (2014); (2) Kawka & Vennes (2012a); (3) Kawka & Vennes (2012b); (4) Kawka et al. (2007); (5) This work; (6) Zuckerman et al. (2003); (7) Kawka & Vennes (2011); (8) Farihi et al. (2011); (9) Farihi et al. (2018); (10) Zuckerman et al. (2011)

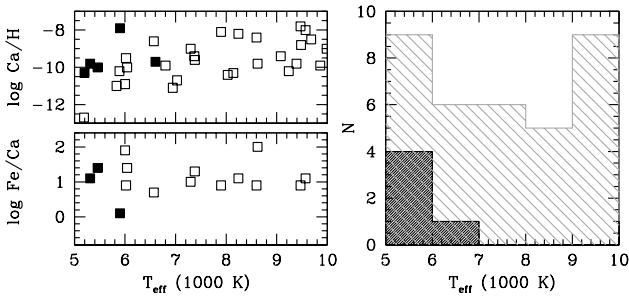


**Figure 5.** (Left:) The abundances of cool DAZ white dwarfs showing  $\log(\text{Ca}/\text{H})$  (top) and  $\log(\text{Fe}/\text{Ca})$  (bottom). The magnetic white dwarfs are shown with full squares and non-magnetic with open squares. (Right:) The temperature distribution of known DAZ white dwarfs with  $T_{\text{eff}} < 10000$  K are shown grey with the magnetic DAZ white dwarfs in grey.

star’s giant phase of evolution. The accretion of rocky planets and asteroids pollutes white dwarfs, but should a giant gaseous planet (a super-Jupiter) were to be present and accreted by the white dwarf, a magnetic field could also be generated as a result and a magnetic DAZ (or DZ) white dwarf would be born.

## 5 SUMMARY

We have presented a spectroscopic analysis of NLTT 7547 showing that it is a new member of the population of cool and magnetic DAZ white dwarfs. With this addition we have shown that the incidence of magnetism is approximately 50% for DAZ white dwarfs with  $T_{\text{eff}} < 6000$  K which decreases significantly to  $\approx 15\%$  for  $6000 < T_{\text{eff}} < 7000$  K and to a virtually zero incidence above 7000 K. A single magnetic DAZ white dwarf, WD2105-820, is known to have a higher temperature ( $T_{\text{eff}} = 10800$  K, Landstreet et al. 2012). The higher incidence is, in part, accounted for by the increasing number of magnetic white dwarfs with age. Other mechanisms are required to explain the sharp increase in the incidence of magnetism in cool polluted white dwarfs. Kawka & Vennes (2014) argued that the phenomenon coincides with the likely presence of a perennially crowded circumstellar environment which may have been caused by the same event that generated the magnetic field.

The kinematics prescribed a membership to the old thin disc or to the thick disc in agreement with a total age of 10 to 13 Gyr inferred from a likely progenitor mass of 0.95 to 1.1  $M_{\odot}$ . Subtracting 0.7 Gyr to the total age of the star, as would be mandated by shorter cooling ages of magnetic white dwarfs similar to NLTT 7547, does not alter our conclusions concerning its population membership.

Challenges were encountered in the computation of cool, radiative atmospheres. The steep temperature gradient resulting from the suppression of convective energy transport is accompanied by a density reversal at the bottom of the atmosphere which could give rise to Rayleigh-Taylor instabilities. This eventuality was not explored further and future work should examine in detail the consequences of this phenomenon on the atmospheric structure. Remaining difficulties in reconciling stellar parameter measurements based on Balmer line profiles and the SED as well as inconsistent calcium abundance measurements require renewed modelling efforts aimed at resolving the competing effect of magnetic field and convective motion.

## ACKNOWLEDGEMENTS

AK and SV acknowledge support from the Czech Science Foundation (15-15943S) and from the Mathematical Sciences Research Visitor Program of the Australian National University. EP acknowledges support from the Ministry of Education of the Czech Republic grant LG15010 and Czech Science Foundation grant GA16-01116S. The International Centre for Radio Astronomy Research is a joint venture between Curtin University and the University of Western Australia, funded by the state government of Western Australia and the joint venture partners. This work has made use of the VALD database, operated at Uppsala University, the Institute of Astronomy RAS in Moscow, and the University of Vienna. This study is based on observations made with ESO telescopes at the La Silla Paranal Observatory under programmes 095.D-0311 and 099.D-0661. This is based in part on data collected with the Danish 1.54-m telescope at the ESO La Silla Observatory. We thank Dayal Wickramasinghe for stimulating discussions. We thank the referee Dr. Stefano Bagnulo for useful comments.

## REFERENCES

- Achilleos N., Wickramasinghe D. T., 1989, *ApJ*, 346, 444
- Albareti F. D. et al., 2017, *ApJS*, 233, 25
- Bagnulo S., Landstreet J. D., Martin A. J., Valyavin G., 2018, *Contrib. Astron. Obs. Skalnaté Pleso*, 48, 236
- Bagnulo S., Landstreet J. D., 2018, *A&A*, 618, A113
- Barklem P. S., Collet R., 2016, *A&A*, 588, A96
- Barklem P. S., Piskunov N., O'Mara B. J., 2000, *A&A*, 363, 1091
- Barstow M. A., Jordan S., O'Donoghue D., Burleigh M. R., Napiwotzki R., Harrop-Allin M. K., 1995, *MNRAS*, 277, 971
- Bédard A., Bergeron P., Fontaine G., 2017, *ApJ*, 848, 11
- Benvenuto O. G., Althaus L. G., 1999, *MNRAS*, 303, 30
- Braithwaite J., Spruit H. C. 2004, *Nature*, 431, 819
- Briggs G. P., Ferrario L., Tout C. A., Wickramasinghe D. T., 2018, *MNRAS*, 478, 899
- Brinkworth C. S., Burleigh M. R., Lawrie K., Marsh T. R., Knigge C., 2013, *ApJ*, 773, 47
- Brown A. G. A. et al., 2018, *A&A*, 616, A1
- Burleigh M. R., Jordan S., Schweizer W., 1999, *ApJ*, 510, L37
- Cheng L., Gauss J., Ruscic B., Armentrout P. B., Stanton J. F., 2017, *J. Chem. Theory Comput.*, 13, 1044
- D'Antona F., Mazzitelli I., 1975, *A&A*, 42, 127
- Debes J. H., Kilic M. 2010, *American Institute of Physics Conference Series*, 1273, 488
- Debes J. H., Sigurdsson S., 2002, *ApJ*, 572, 556
- Dufour P., Vornanen T., Bergeron P., Fontaine G., Berdyugin A., 2013, 18th European Workshop on White Dwarfs, ASP Conf. Ser., Vol. 469, eds. J. Krziesiński, G. Stachowski, P. Moskalik, K. Bajan, 167
- Dunlap B. H., Clemens J. C., 2015, in ASP Conf. Ser., Vol. 493, eds. P. Dufour, P. Bergeron, G. Fontaine, 547
- Euchner F., Reinsch K., Jordan S., Beuermann K., Gänsicke B. T., 2005, *A&A*, 442, 651
- Farihi J., Dufour P., Napiwotzki R., Koester D. 2011, *MNRAS*, 413, 2559
- Farihi J., et al., 2018, *MNRAS*, 474, 947
- Farihi J., Zuckerman B., Becklin E. E., 2008, *ApJ*, 674, 431
- Ferrario L., de Martino D., Gänsicke B. T., 2015, *Space Sci. Rev.*, 191, 111
- Ferrario L., Vennes S., Wickramasinghe D. T., Bailey J. A., Christian D. J., 1997, *MNRAS*, 292, 205
- Ferrario L., Wickramasinghe D., Liebert J., Williams K. A., 2005, *MNRAS*, 361, 1131
- García-Berro E., et al., 2012, *ApJ*, 749, 25
- Gentile Fusillo N. P., Tremblay P.-E., Jordan S., Gänsicke B. T., Kalirai J. S., Cummings J., 2018, *MNRAS*, 473, 3693
- Giammichele N., Bergeron P., Dufour P., 2012, *ApJS*, 199, 29
- Hogg D. W., Blanton M. R., Roweis S. T., Johnston K. V., 2005, *ApJ*, 629, 268
- Hollands M. A., Gänsicke B. T., Koester D., 2015, *MNRAS*, 450, 681
- Hollands M. A., Gänsicke B. T., Koester D., 2018, *MNRAS*, 477, 93
- Hollands M. A., Koester D., Alekseev V., Herbert E. L., Gänsicke B. T. 2017, *MNRAS*, 467, 4970
- Johnson D. R. H., Soderblom D. R., 1987, *AJ*, 93, 864
- Jura M., 2008, *AJ*, 135, 1785
- Jura M., Farihi J., Zuckerman B., 2007, *ApJ*, 663, 1285
- Kawka A., Briggs G. P., Vennes S., Ferrario L., Paunzen E., Wickramasinghe D. T., 2017, *MNRAS*, 466, 1127
- Kawka A., Vennes S., 2006, *ApJ*, 643, 402
- Kawka A., Vennes S., 2011, *A&A*, 532, A7
- Kawka A., Vennes S., Dinnbier F., Cibulková H., Németh P. 2011, *American Institute of Physics Conference Series*, 1331, 238
- Kawka A., Vennes S., 2012a, *MNRAS*, 425, 1394
- Kawka A., Vennes S., 2012b, *A&A*, 538, A13
- Kawka A., Vennes S., 2014, *MNRAS*, 439, L90
- Kawka A., Vennes S., 2016, *MNRAS*, 458, 325
- Kawka A., Vennes S., Schmidt G.D., Wickramasinghe D.T., Koch R., 2007, *ApJ*, 654, 499
- Kemic S. B., 1975, *Ap&SS*, 36, 459
- Kepler S. O. et al., 2013, *MNRAS*, 429, 2934
- Kilic M., von Hippel T., Leggett S. K., Winget D. E., 2006, *ApJ*, 646, 474
- Kilic M., et al., 2017, *ApJ*, 837, 162
- Landi Degl'Innocenti E., Landolfi M., 2004, *Polarisation in spectral lines*, No. 307 in *Astrophysics and Space Library*, Kluwer Academic Publishers, Dordrecht ASSL, 307
- Landstreet J. D., Bagnulo S., Valyavin G. G., Fossati L., Jordan S., Monin D., Wade G. A., 2012, *A&A*, 545, A30
- Landstreet J. D., Bagnulo S., Valyavin G. G., Valeev A. F., 2017, *A&A*, 607, A92
- Lawrie K. A., Burleigh M. R., Dufour P., Hodgkin S. T., 2013, *MNRAS*, 433, 1599
- Liebert J., Sion, E. M., 1979, *ApJ*, 20, L53
- Liu W. M., Chaboyer B., 2000, *ApJ*, 544, 818
- Martin B., Wickramasinghe D. T., 1984, *MNRAS*, 206, 407
- Maxted P. F. L., Ferrario L., Marsh T. R., Wickramasinghe D. T., 2000, *MNRAS*, 315, L41
- Pauli E.-M., Napiwotzki R., Altmann M., Heber U., Odenkirchen M., Kerber F., 2003, *A&A*, 400, 877
- Romero A. D., Campos F., Kepler S. O., 2015, *MNRAS*, 450, 3708
- Rossi L. J., 2015, *A&C*, 12, 11
- Salaris M., Held E. V., Ortolani S., Gullieuszik M., Momany Y., 2007, *A&A*, 476, 243
- Salim S., Gould A., 2003, *ApJ*, 582, 1011
- Sauval A. J., Tatum J. B., 1984, *ApJS*, 56, 193
- Sayres C., Subasavage J. P., Bergeron P., Dufour P., Davenport J. R. A., AlSayyad Y., Tofflemire B. M., 2012, *AJ*, 143, 103
- Schimeczek C., Wunner G., 2014, *ApJS*, 212, 26
- Schmidt G. D., Smith P. S., 1995, *ApJ*, 448, 305
- Skrutskie M. F. et al., 2006, *AJ*, 131, 1163
- Soubiran C., Bienaymé O., Siebert A., 2003, *A&A*, 398, 141
- Subasavage J. P., Henry T. J., Bergeron P., Dufour P., Hambly N. C., Beaulieu T. D., 2007, *AJ*, 134, 252
- Subasavage J. P., Jao W.-C., Henry T. J., Bergeron P., Dufour P., Ianna P. A., Costa E., Méndez R. A., 2009, *AJ*, 137, 4547
- Subasavage J. P., et al., 2017, *AJ*, 154, 32
- Tremblay P.-E., Fontaine G., Freytag B., Steiner O., Ludwig H.-G., Steffen M., Wedemeyer S., Brassard P., 2015, *ApJ*, 812, 19
- Valyavin G., Wade G. A., Bagnulo S., Szeifert T., Landstreet J. D., Han I., Burenkov A., 2008, *ApJ*, 683, 466
- Valyavin G., et al., 2014, *Nature*, 515, 88
- Valyavin G., Fabrika S., 1999, 11th European Workshop on White Dwarfs, ASP Conf. Ser., Vol. 169, eds. S.-E. Solheim, E.G. Meistas, 206
- Vennes S., Kawka A., 2013, *ApJ*, 779, 70
- Vennes S., Kawka A., Ferrario L., Paunzen E., 2018, *CoSka*, 48, 307
- Vennes S., Schmidt G. D., Ferrario L., Christian D. J., Wickramasinghe D. T., Kawka A., 2003, *ApJ*, 593, 1040
- Vernet J. et al., 2011, *A&A*, 536, A105
- Wende S., Reiners A., Seifahrt A., Bernath P. F., 2010, *A&A*, 523, A58
- Wickramasinghe D. T., Martin B., 1986, *MNRAS*, 223, 323
- Williams K. A., Montgomery M. H., Winget D. E., Falcon R. E., Bierwagen M., 2016, *ApJ*, 817, 27
- Zuckerman B., Koester D., Reid I. N., Hüensch M. 2003, *ApJ*, 596, 477
- Zuckerman B., Melis C., Klein B., Koester D., Jura M., 2010, *ApJ*, 722, 725
- Zuckerman B., Koester D., Dufour P., Melis C., Klein B., Jura M. 2011, *ApJ*, 739, 101

This paper has been typeset from a  $\text{\LaTeX}$  file prepared by the author.